Proc. Ind. Assoc. Cult. Sci. **77B** (5), p1–p10 (1994)

I J P B
— an international journal

The radio and X-ray views of the Sun : an approach to modern solar physics*

M R Kundu
Department of Astronomy, University of Maryland, College Park, Maryland, USA

Received 15 July 1994

Abstract : Over the past several years, space missions such as the Solar Maximum Mission (SMM), Compton Gamma Ray Observatory (CGRO), the Japanese Solar Satellite Yohkoh along with large ground based radio facilities such as the University of Maryland Clarke Lake Radio Observatory (CLRO), the Very Large Array (VLA) and the Berkeley-Illinois-Maryland Millimeter Array (BIMA) have provided high spatial resolution (seconds of arc) and high temporal resolution (fraction of a second) images of solar flares and other eruptive phenomena over a wide range of wavelengths—from gamma rays through visible light to radio. These imaging observations have provided new insights to our understanding of energetic phenomena on the Sun, with particular reference to coronal mass ejection (CME) events and the production of MeV-energy electrons in solar flares. In this paper, we present samples of different solar phenomena : coronal mass ejection events as observed with space-borne coronagraph in conjunction with the Clarke Lake Radio Observatory (CLRO) multifrequency radioheliograph operating at low frequencies 25–125 MHz, the MeV-energy electrons as detected with the BIMA telescope operating at millimeter wavelengths and the gamma-ray experiments aboard the Gamma Ray Observatory

Keywords : Solar physics, radio and X-ray views

PACS Nos. : 96.60. Pb, 96.60. Rd

1. Introduction

In recent years, many large radio interferometers have been built, primarily for cosmic research. Their operating wavelengths range from meter to centimeter and millimeter wavelengths. These ground-based instruments have been used to a limited extent for solar radio research often independently and sometimes in conjunction with several space missions such as the Solar Maximum Mission (SMM), the Japanese Solar Satellite Yohkoh, and the primarily cosmic mission Compton Gamma Ray Observatory (CGRO). These space missions

*Santanu Ghosh Memorial Lecture 12th delivered at the Indian Association for the Cultivation of Science, Calcutta on 17 December 1993

Text and references have been composed as per author's style.

carried instruments, both imaging as well as spectrometric over a wide spectral range from ultra-violet and soft X-rays to hard X-rays and gamma-rays. The availability of observations in different spectral domains permit us to sample the solar flare plasma from cool to very high temperatures, or from low energy to very high energies.

In the Sun's atmosphere, the emission at different radio frequencies originate from different levels of the Sun's atmosphere, the highest frequencies or shortest wavelengths come from the lowest levels and lower frequencies from the higher levels. The electron density and therefore the plasma critical frequency decreases with height from the photosphere, [a wave of frequency f can escape only if $f > f_0$ where f_0 (plasma critical frequency) in MHz $= 9 \times 10^{-3} \sqrt{N}$, N = electron density cm^{-3}] with the consequence that we can explore different regions of the Sun's atmosphere by using different frequencies or wavelengths. Thus, if we want to study the origin of solar flares whose energy release takes

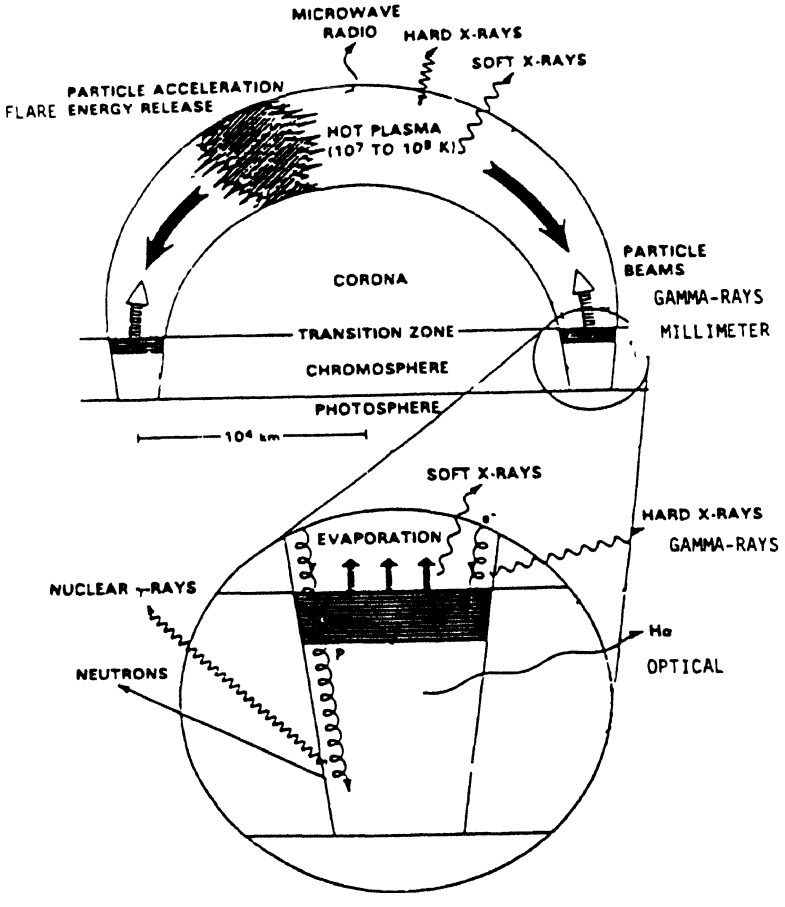

Figure 1. A schematic solar flare model showing the locations of various emissions in a simple flaring loop.

place in the chromosphere and the low corona, centimeter and millimeter wavelengths are the most appropriate wavelengths to be used, whereas if we are interested in studying mass

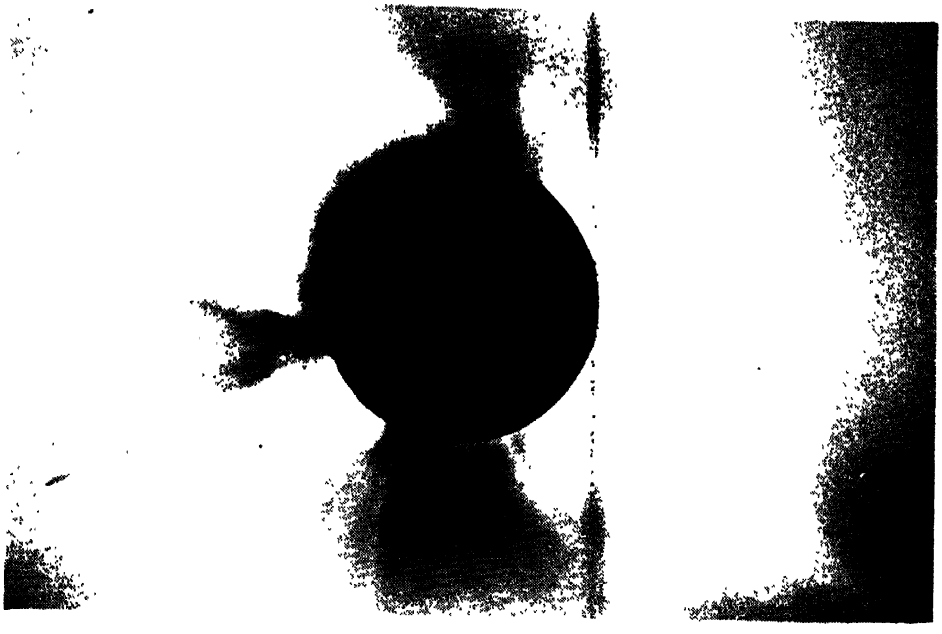

Figure 2. A white light picture of the total solar eclipse of July 11, 1991. Note the coronal streamers and rays.

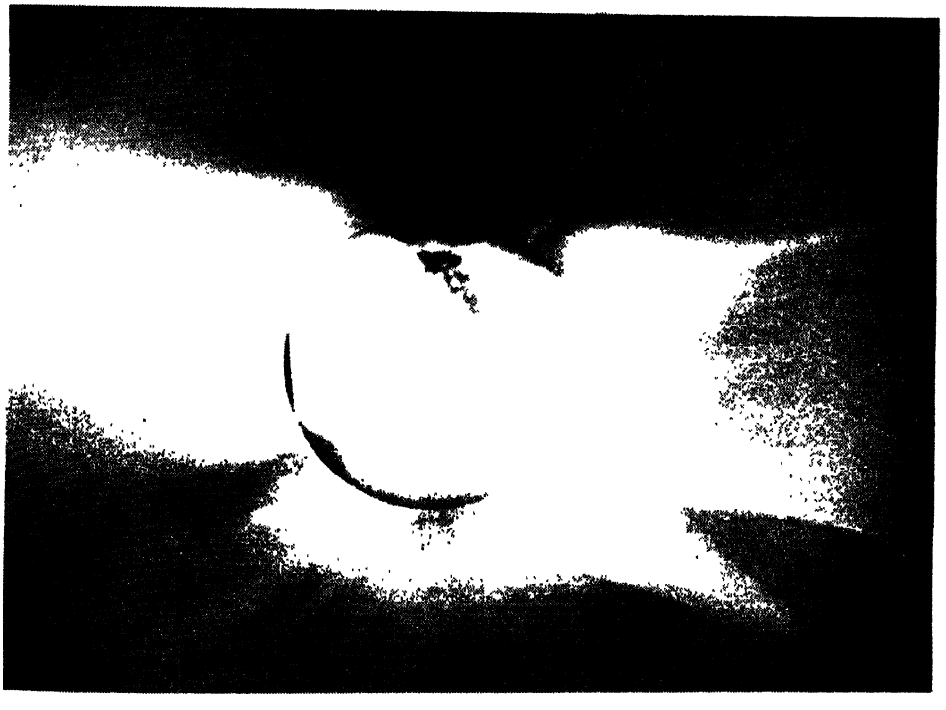

Figure 3. A white light coronagraph image of the Sun taken from the Skylab-ATM mission in 1973. Note the coronal streamers and other structures which are strikingly similar to those in a total eclipse picture. Also shown is the disk image observed in a spectral line.

Plate II

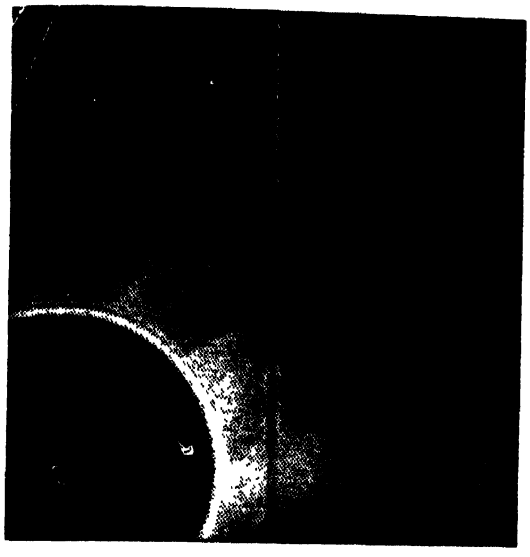

OCT 24, 1989 15:23

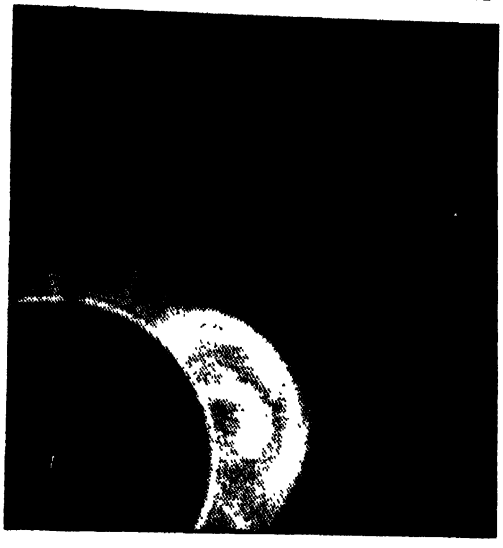

OCT 24, 1989 18:09

OCT 24, 1989 18:25

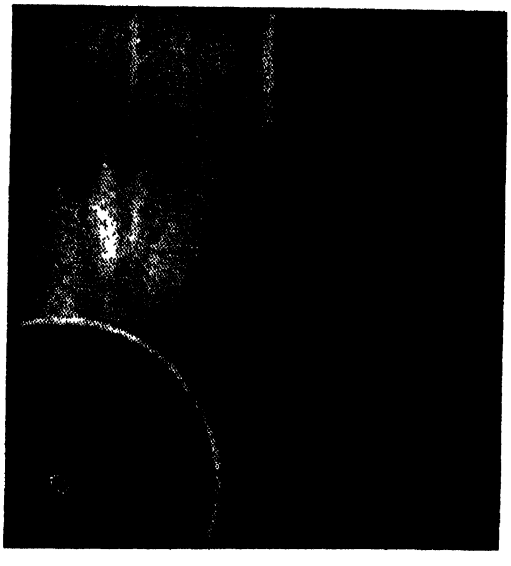

OCT 24, 1989 19:15

Figure 4. A time sequence of 4 SMM coronagraph images showing the development of a CME event. Note that the pre-existing structures are blown out by the passage of the event. The coronal material, visible above the occulting disk in the lower right center of the image at 15 : 23, is blown out by 19 : 15 due to the loop/cavity appearing in the intervening images (SMM coronagraph picture).

Plate III

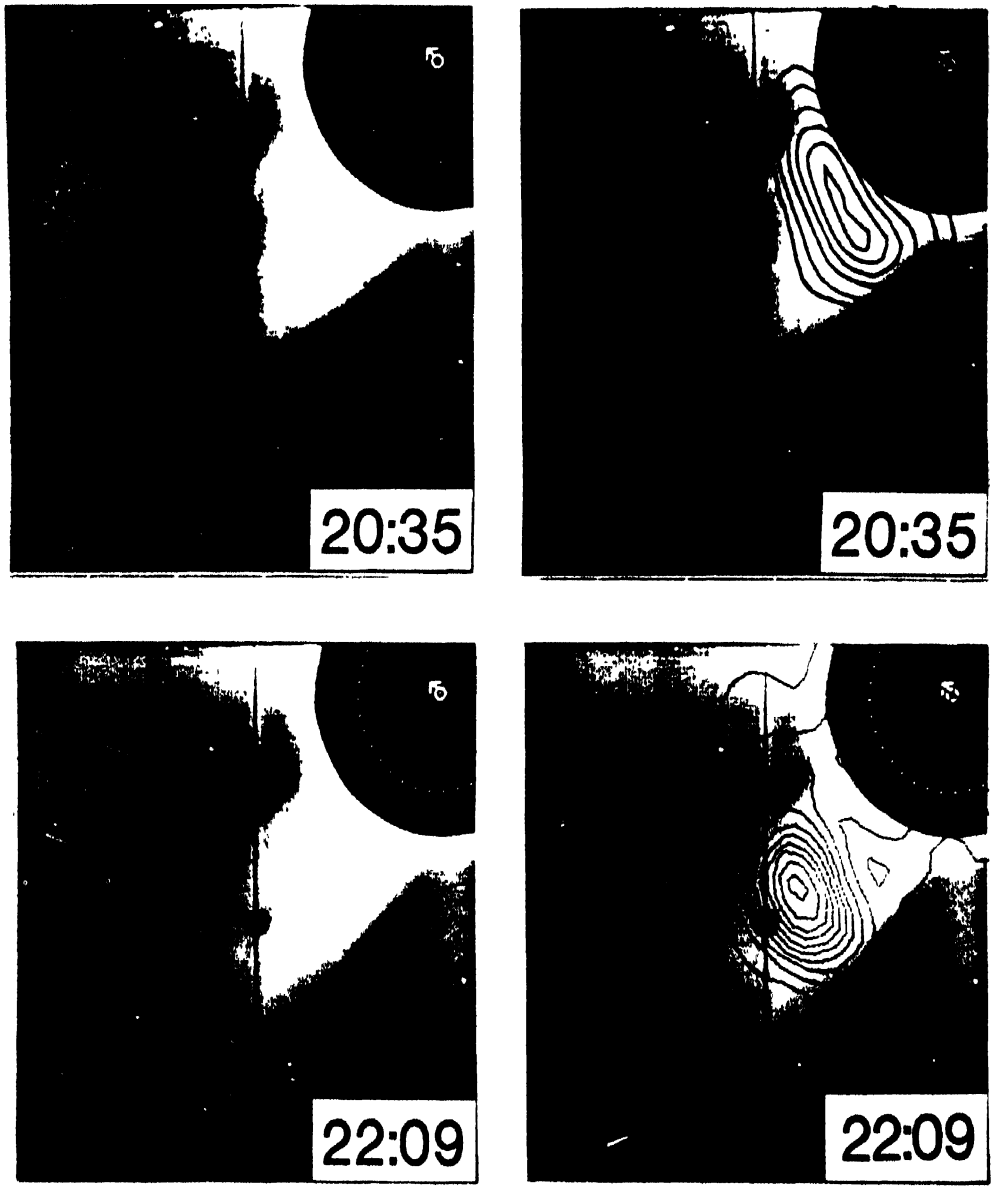

Figure 5. (a) Superposition (right) of type II-moving type IV bursts on the SMM C/P image at 20 : 35 UT (left). (b) Superposition (right) of the moving type IV burst toward its end on the SMM C/P image at 22 : 09 UT. The arrow mark corresponds to solar north (After Kundu *et al* 1989).

motions, propagation of particle streams in the corona and the interplanetary medium, meter and decameter wavelengths are more appropriate.

In this paper, we'll discuss two different solar phenomena : coronal mass ejection (CME) events as observed with SMM and CLRO radioheliograph; and high energy solar flare emissions as obtained from radio millimeter, X-ray and gamma-ray observations using the BIMA telescope, Yohkoh and GRO missions. We'll attempt to present these data in the context of presently existing flare models.

To understand the radio, X-ray, gamma-ray and other electromagnetic emissions, we consider a simple working model (Figure 1) in which energy release occurs in the corona, and it accelerates nonthermal electrons. These propagate down magnetic field lines, strike the chromosphere and produce hard X-rays and gamma-ray continuum by thick-target bremsstrahlung. The nonthermal electrons deposit their energy in the chromosphere as heat. The heated, dense chromospheric material produces the flare *H*-alpha emission and rises up into the corona, fills magnetic loops, expands and produces soft X-rays. Soft X-ray observations show large-scale loops at temperatures of millions to several tens of millions of degrees K, covering a much larger area than the original footpoints where nonthermal energy is deposited.

2. Observations in visible light of coronal mass ejection events

The Sun as we see it in visible light is really the Sun's photosphere. The Sun's corona is transparent to visible light, we see it during total solar eclipse by Thompson Scattered light. Figure 2 shows an excellent picture of the Sun's corona taken during the total solar eclipse of July 11, 1991. One sees clearly the large scale coronal structures such as streamers and rays. Pictures like this are presently taken routinely by coronagraphs aboard spacecrafts (Skylab, SMM and upcoming SOHO) (see Figure 3).

3. Coronagraph pictures of CME phenomena

Coronagraph images reveal coronal features in light radiated from the solar photosphere hidden behind the occulting disk and scattered into the instrument by electrons in the corona. Brightness of any feature in such images is related to the density of the ionized coronal plasma. The outermost bright loop-like feature (Figure 4) moving outward with velocities of several hundred km s^{-1} suggest ejection of material from the Sun, hence the common name for this phenomenon : CME. Typical mass of a CME event is ~10^{16} g. Its average speed is ~400 km/s; maximum speed is > 1000 km/s (flare-associated); and minimum speed is ~20 km/s (associated with streamer evolution).

A CME phenomenon is characterized by the presence of a dark cavity within a bright frontal loop. It has a bright central core suggesting prominence or other chromospheric material. The dark cavity (Figure 4) appears to be the unifying feature common to most mass ejections with a simple observable structure; the major variability seems to be in the appearance of surrounding bright loop and embedded bright core.

The dark cavity is a region of low density but strong magnetic fields and is considered to be the prominence cavity (in ejections associated with eruptive prominences); it rises and deforms the overlying corona into a surrounding bright loop as it moves outward and is probably responsible for the initiation of the entire phenomenon because of its buoyancy in the background atmosphere.

4. Onset of mass ejection

Prominence cavities are regions of low coronal density and so should be buoyant relative to the surrounding coronal plasma. They are held in equilibrium by magnetic tension in an arcade of field lines that permeate them; closing over a magnetic neutral line thought to lie beneath the prominence. Examination of idealized models of this equilibrium show that it exists only for limited ranges of parameters such as the size of cavity or magnetic flux contained in it. If slow evolution of the magnetic field were to lead out of the range where tension can contain cavity, it should rise buoyantly through the corona giving rise to a mass ejection. Any features contained by fields within the cavity, such as a prominence, should rise with it. A prominence eruption could be associated with such an event. As mentioned earlier, the average speed of all CME's is ~400 km s^{-1}. The prominence-associated CME's have average speed of ~330 km s^{-1}; and the flare-associated CME's have average speed of ~775 km s^{-1}. The average speeds of CME's associated with flares and radio bursts are similar. Both flares and CME's can produce shocks which may result in type II bursts.

A flare explosion produces a finite amplitude compressive MHD disturbance which steepens into a shock while propagating away from the flare site. How fast the MHD disturbance steepens into a shock depends on the rate of energy input into the disturbance and its speed relative to the ambient characteristic speed of the coronal medium. The relative characteristic speed is the Alfvén speed, ~500–1000 km/s.

The outer structure of a CME is due to the disruption of equilibrium of a large scale magnetic structure. The CME phenomenon is identified as the dark magnetic cavity within which one observes H_α material either from the flare or prominence eruption. The initiation and formation of features in CMEs are related to closed magnetic structures in the large scale coronal magnetic field. Disruption of these closed magnetic structures leads to a 'blown-open' region in the corona, with material originally contained within the closed structures, from the low corona or the chromosphere (prominence) ejected from the Sun. That is, a large closed magnetic structure is changed to an open structure by the mass ejection. Disruption of a large scale coronal magnetic structure related to mass ejection persists on time scales of hours to days. The mass ejection process thus is related not only to large scale equilibrium of coronal structure, but it is possible that it provides a mechanism by which that structure changes.

5. Radio signatures of coronal mass ejection

One expects radio emission to be associated with CME's because the latter produce shocks. Observations of CME's during the Skylab era had led to the following conclusions (Gosling *et al* 1976) : If $V_{CME} < 400$ km/s, no type II or type IV burst emission is associated with the

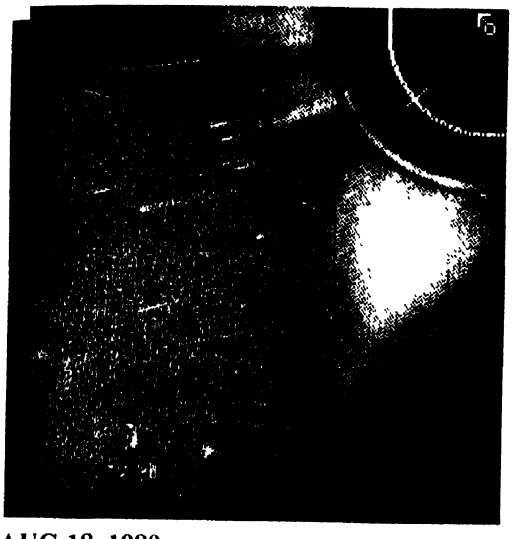

AUG 18, 1980 11:43

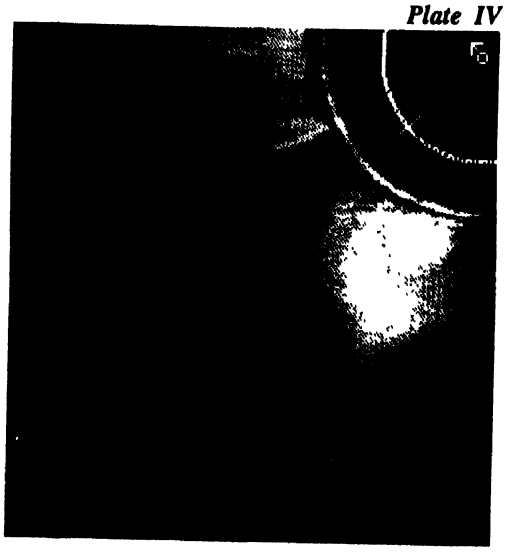

11:54

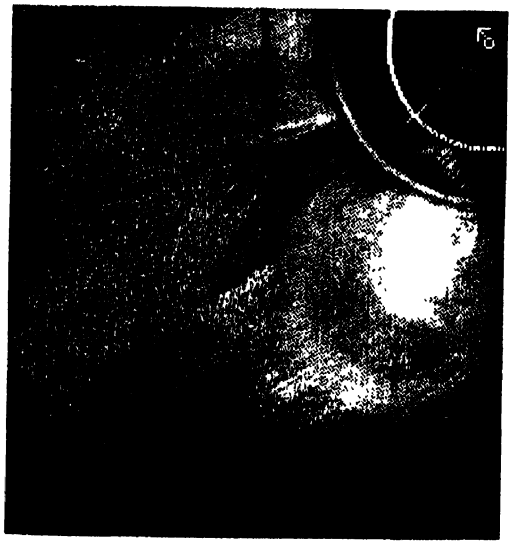

12:15

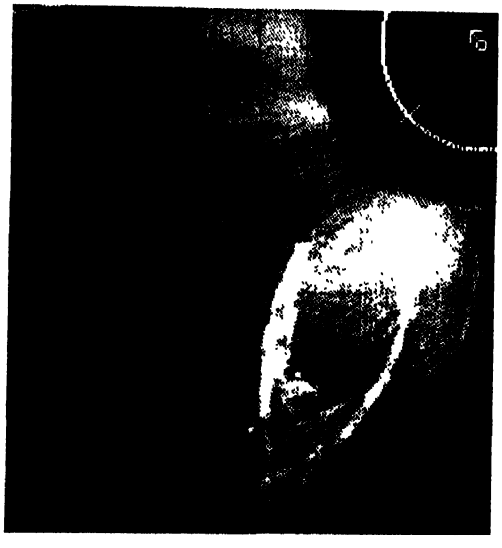

13:10

Figure 6a. A time sequence of four SMM coronagraph images (in the same format as Figure 4 showing the formation of a coronal mass ejection on August 18, 1980 (SMM coronagraph picture).

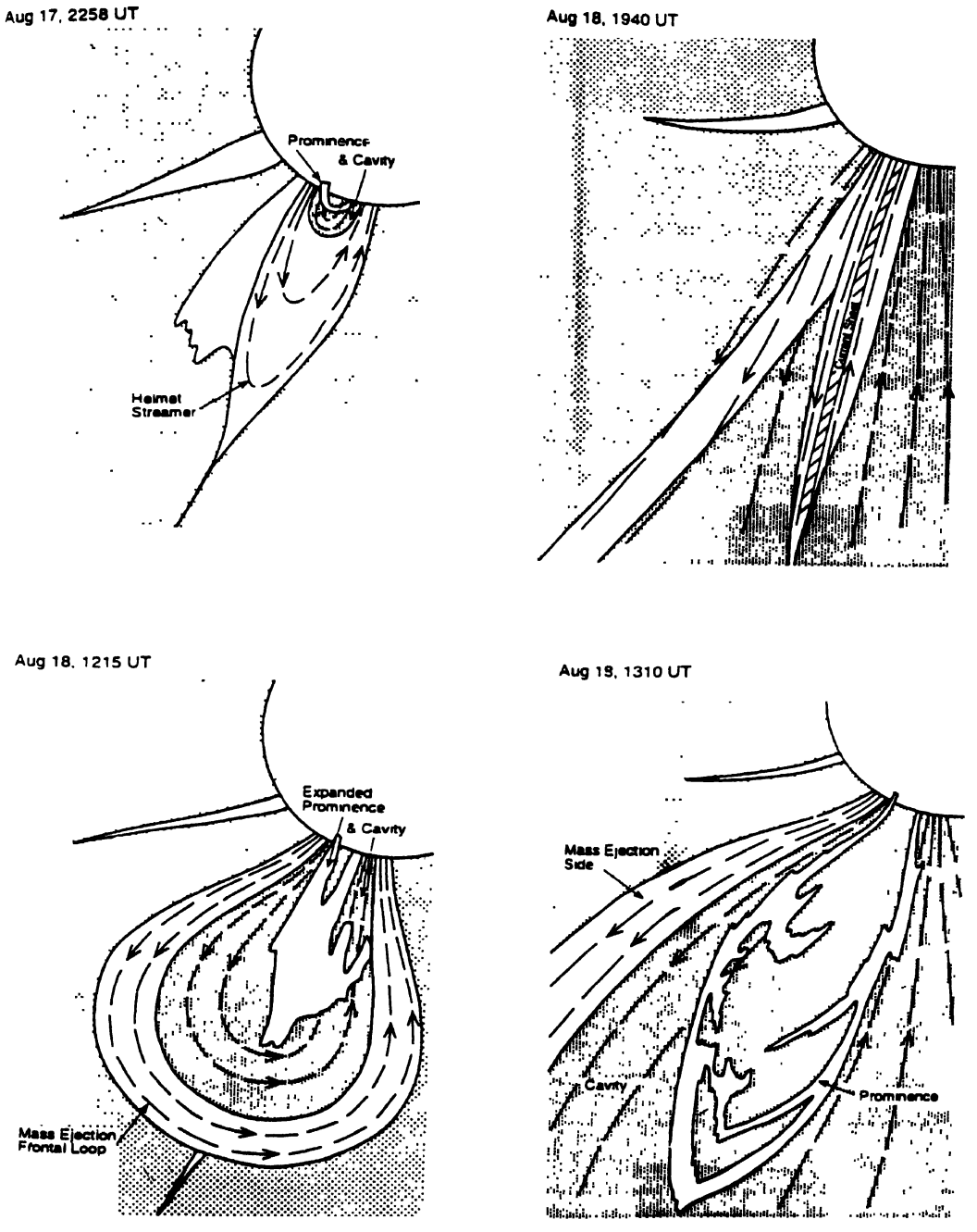

Figure 6b. A magnetic interpretation of formation of the loop-like mass ejection shown in Figures 4, 5 and 6a. The (dashed) closed magnetic field lines sketched on a cross section of a helmet streamer are frozen into the plasma. They must then be distorted into extended loops as the ejection forms. The tops of these loops are drawn away from the Sun leaving a region that looks to be magnetically open and that contains a vertical current sheet separating magnetic fields of opposite polarity (SMM coronagraph picture).

CME; (2) If 400 km/s < V_{CME} < 700 km/s, either a type II or a type IV can be associated with the CME; (3) If V_{CME} > 700 km/s, a type II–type IV pair can be associated with the CME. (Note that a type II burst is indicative of shocks in the sun's atmosphere, while type IV burst emission indicates the existence of a plasmoid). The above conclusions were primarily based upon temporal associations and only occasionally on simultaneous radio imaging and white light coronagraph observations. High spatial resolution (of the order of a few arc minutes at meter-decameter wavelengths) imaging observations with the CLRO radioheliograph simultaneously with the SMM coronagraph observations have shown that it is possible to observe radio emission of type II and type IV during slow CME's (V < 200 km/s). Figure 5 shows the results of analysis of one such slow CME event (Kundu *et al* 1989). Recently, we found evidence that nonthermal radio emission can sometimes be associated with a coronal disconnection event as believed to be the case for an event observed by CLRO and SMM instruments (Gopalswamy *et al* 1994). Coronal disconnection events constitute a class of CME's in which a coronal structure detaches from the sun, appearing as a U or V-shaped feature in white light coronagraph images. These events are probably evidence for reconnection in the corona, and they may be responsible for maintaining the interplanetary magnetic field at a relatively constant level. The reconnection may also be responsible for acceleration of particles responsible for the observed nonthermal radio emission. This is illustrated in Figure 6.

6. Millimeter – gamma ray emission

The Sun's corona is transparent to mm-λ emission and does not contribute to opacity in the mm domain. Nature of sources one sees at mm-λ depends on the emission mechanism. During flares, very energetic electrons can be present which radiate gyrosynchrotron emission at high harmonics of the gyrofrequency; during 'quiet' periods strongest source of opacity is due to thermal bremsstrahlung from cool material in the chromosphere.

Since typical gyrofrequency in the lower corona over active regions is ~ 1–5 GHz, radiation at 86 GHz is at high harmonics, and we only have significant opacity if there are MeV electrons present. Even if there is a 50 keV thermal source present in 1000 gauss magnetic fields, we won't see any gyrosynchrotron emission at millimeter wavelengths although strong microwave radiation will be seen.

The emission of solar flares at millimeter wavelengths is of great interest both in its own right and because it is generated by the very energetic electrons which also emit gamma rays. Since high-resolution imaging at gamma-ray energies is not presently possible, millimeter observations can act as a substitute. In addition, the millimetric emission is undoubtedly optically thin (except possibly for a small class of very large flares which have spectra rising beyond 100 GHz; Kaufmann *et al* 1985), and thus is not subject to the same ambiguities of interpretation which are prevalent in the study of solar microwave bursts.

The observations reported here were made in June 1991 during a GRO campaign with the Berkeley-Illinois-Maryland Millimeter Array (BIMA); at that time it consisted of only three elements, which was not adequate for mapping highly variable solar phenomena, but was

excellent for studies of the temporal structure of flares at millimeter wavelengths at several different spatial scales (Kundu *et al* 1992; Kundu *et al* 1994). Our observations represented an improvement of an order of magnitude in both sensitivity and spatial resolution compared with previous solar observations at these wavelengths. Figure 7(a) presents the GRO-BATSE

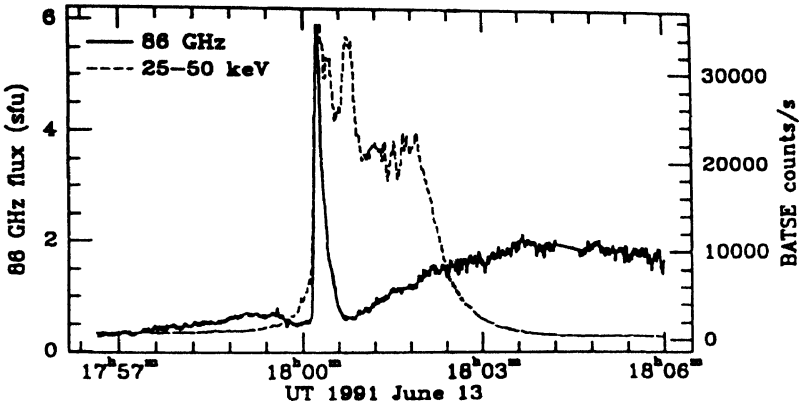

Figure 7a. Comparison of the time profiles of the 1991 June 13 18 UT flare emission in 25–50 keV hard X-rays and the 86 GHz (After Kundu *et al* 1992)

(Burst and Transient Spectrometer Experiment) data along with 86 GHz data for a burst observed on June 13, 1991, ~ 17:57–18:06 UT. The flare evolution is shown for the lowest BATSE energy channel, 25–50 keV. In Figure 7(b) we have plotted the time profile of the

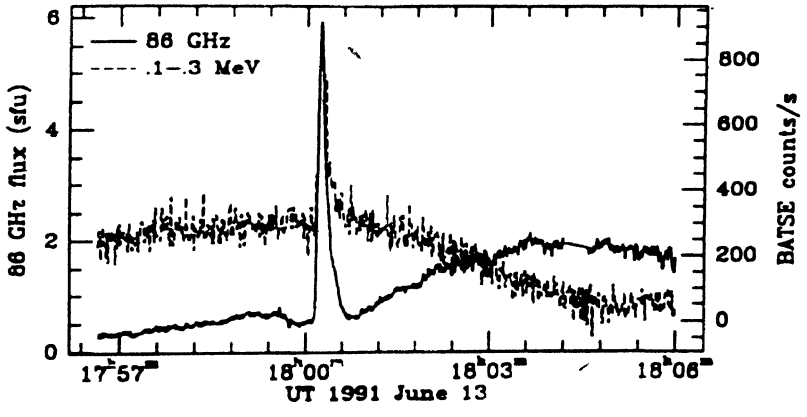

Figure 7b. Comparison of the time profiles of the 1991 June 13 18 UT flare emission in the 100–300 keV hard X-rays seen by BATSE (broken line) and the 86 GHz emission recorded by BIMA (solid line) (After Kundu *et al* 1992).

BATSE 0.1–0.3 MeV channel and the BIMA 86 GHz profile to the same scale. There were no significant counts above the background in the 0.3–1 MeV channel. The remarkable feature of this flare is that while the overall profile in the 25–50 keV range is relatively simple, with a sharp rise to a plateau level containing a number of sub-peaks followed by a rapid

decay, in the higher-energy channels we see a sharp spike right at the beginning of the flare. We and others (White and Kundu 1992, Ramaty 1969, Ramaty and Petrosian 1972) have argued that millimeter emission in the impulsive phase should be due to gyrosynchrotron emission from the most energetic electrons in a flare, and on this basis one would predict that the millimeter emission would also show a sharp spike in the onset phase. This is exactly what is seen. The close similarity of the 0.1–0.3 MeV and 86 GHz profiles provides convincing evidence that the millimeter emission is indeed due to the most energetic electrons in a solar flare : the same energetic electrons that produce gamma ray continuum. The importance of this result is that we can obtain high-spatial-resolution information on source structures with millimeter-interferometer observations, which is not presently possible directly with gamma-ray observations.

Figure 7(a) also emphasizes that, in addition to the impulsive phase coinciding with the gamma ray emission, the millimeter emission shows an extended component which rises slowly and continues beyond 1806 UT. Thus in this event, we clearly see two easily-distinguishable components in the millimeter emission : an impulsive component coinciding in time with the impulsive gamma ray emission, and a gradual extended component with no gamma ray counterpart. In fact, the 86 GHz profile in this case shows gradual mm burst emission corresponding roughly with the GOES soft X-ray emission (Figure 7(c)). In this case the hard X-ray rise corresponds to the rise phase of both mm and soft X-ray emission. A number of 1991 June flares, both with and without 86 GHz impulsive phases, showed a thermal phase at 86 GHz which was similar in profile to the GOES data, including the 13 June 18 UT event. We also found evidence that for some simple impulsive events with a very sharp rise there is a clear delay of several seconds between the 25–50 keV impulsive rise and the 86 GHz rise (Figure 8). Since we can associate the 86 GHz emission with high-energy

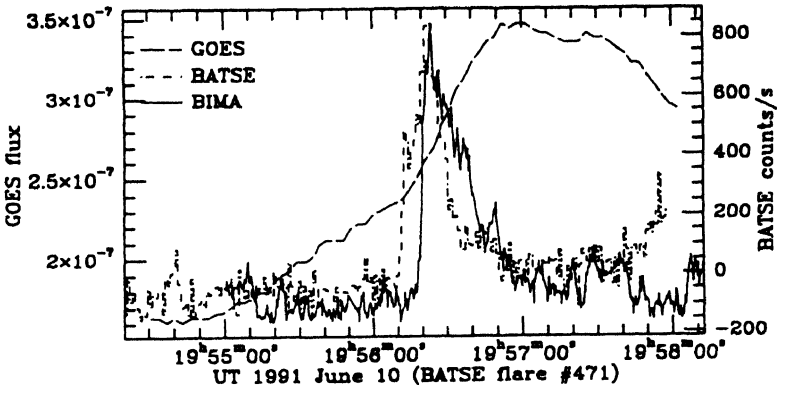

Figure 8. The soft X-ray, hard X-ray and 86 GHz time profiles of a flare at 20 UT on June 10. This small event was not given a GOES classification, and was barely noticeable in the usual log plots of soft X-ray data. It shows a clear delay between the 86 GHz and hard X-ray profiles; the soft X-ray flux begins to rise well before the onset phase in hard X-rays (After Kundu *et al* 1994).

electrons (> 300 keV), the implication is that there is a delay between the production of the 25–50 keV electrons and the > 300 keV electrons. Such delays can be attributed to the need to

Plate V

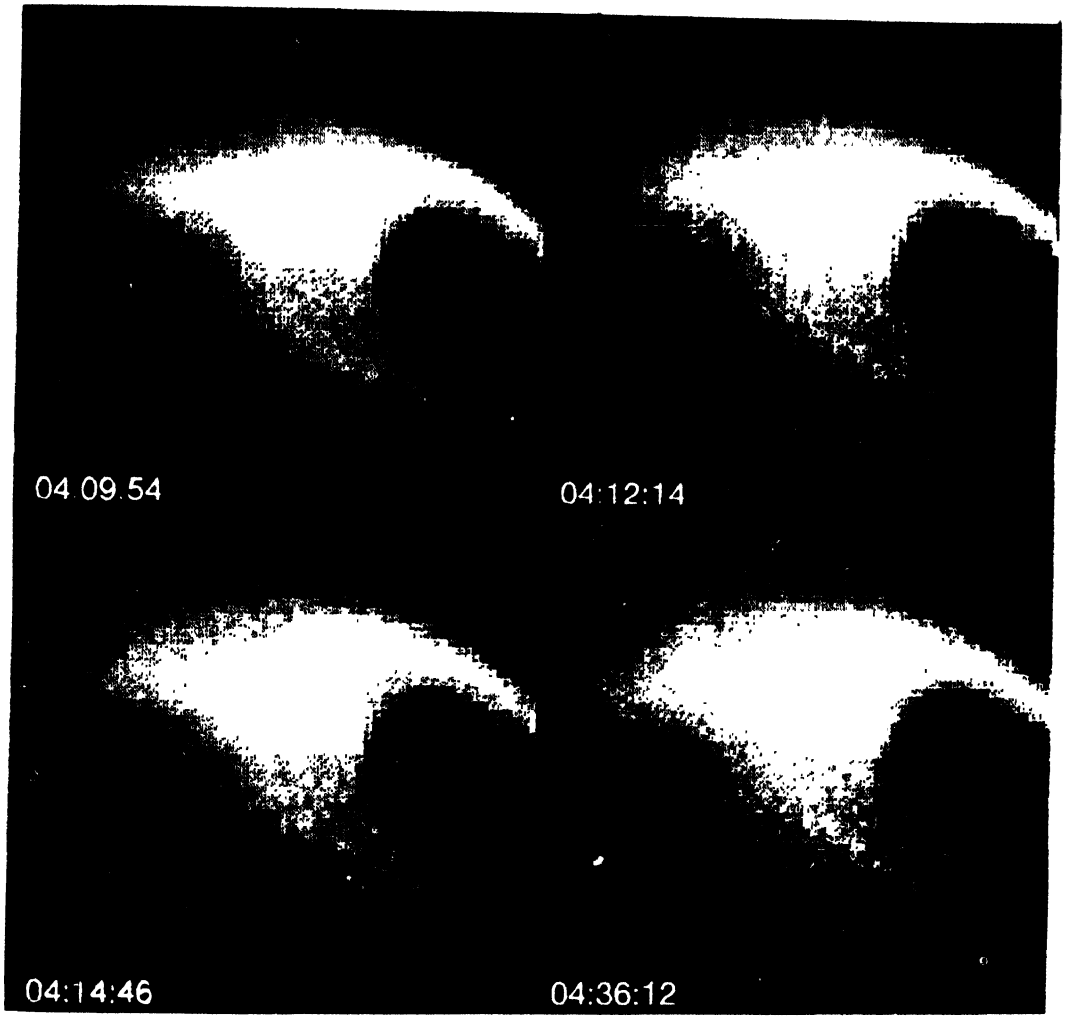

Figure 9. Yohkoh-SXT images with full resolution (2"45 pixels) for the impulsive phase of a limb flare that occurred in a helmet streamer structure (After Tsuneta *et al* 1992).

accelerate electrons from low to high energies, and can be used to constrain candidate emission mechanisms (Kundu *et al* 1992). Since millimeter emission occurs in flares of all sizes, including the most insignificant ones, we can conclude that MeV-energy electrons are generated in flares more abundantly than previously believed.

7. Yohkoh-SXT imaging of flare X-rays

Various flare models have been suggested in the literature to explain radio emission from solar flares (see, *e.g.*, Kundu *et al* 1982). The helmet streamer type flare model was first invoked to explain the existence of metric type III bursts in the corona (Sturrock 1967). This helmet streamer type of magnetic configuration has now been directly observed by Tsuneta *et al* (1992) from Yohkoh SXT observations. Tsuneta *et al* (1992) observed a long-enduring soft X-ray flare at the solar limb by the Soft X-ray Telescope (SXT) aboard the Yohkoh spacecraft from its pre-flare stage through the post-flare phase (Figure 9). A 'helmet streamer' arch appeared several hours prior to the flare, in association with a continuous expansion and restructuring of the active-region magnetic structure. The arch then started to flare, and increased its height and footpoint separation with a velocity of 10–30 km s^{-1}. It is apparently this expansion which triggered the flare. The morphology of the flare arch strongly suggests that the current sheet, thus created, was the primary energy source of the flare. An *X*-type or *Y*-type reconnection point appears to have been formed at the top of the arch. This is further supported by the gradual increase of the flare arch height and the separation as the flare goes on (Hirayama 1974, Pneuman 1981). The temperature structure of the X-ray loop also suggests that the flare energy was supplied by an ongoing reconnection process near the top of the loop or the slow shock front formed by the Petschek type magnetic reconnection (Cargill and Priest 1983). The arch has a complex temperature structure in the rising phase, whereas the outer arches have systematically higher temperatures in the decay phase.

8. Summary conclusions

We have summarized some morphological properties of coronal mass ejection events and their radio signatures at meter-decameter wavelengths. We note that even slow CME's (speed < 200 km/s) can have radio signatures in the form of type II and type IV bursts associated with them. The CME's of 'disconnection' type can sometimes have nonthermal radio emission associated with them.

We have shown that impulsive-phase millimeter burst emission probes MeV electrons produced during flares and MeV electrons are produced in flares of all sizes. There are two phases in millimeter burst emission : a nonthermal impulsive phase and a thermal gradual phase. Both phases are often observed in the same flare. Some flares show no nonthermal impulsive phase at millimeter wavelengths, although they seem to show it at 25–50 keV electrons. These gradual phase flares correspond well to the GOES soft X-ray emission. There appears to exist some delay between BIMA mm-emission onset and BATSE 25–100 keV X-ray emission. Both results have implications in the particle acceleration process.

Yohkoh-SXT imaging observations have provided evidence for helmet streamer type flare mechanism.

References

Cargill, P. J. and Priest, E. R., 1983 *J. Astrophys.* **266** 383

Gopalswamy, N., Kundu, M. R. and St. Cyr, C., 1994 *Ap. J. (Lett.)* (in press)

Gosling, J J., Hildner, E , MacQueen, R. M., Munro, R H., Poland, A. I. and Ross, C. L., 1976 *Solar Phys* **48** 389

Hirayama, T., 1974, *Solar Phys.* **34** 323

Kaufman, P., Correia, E., Costa, J. E. R., Vaz, A. M. Z. and Dennis, B., 1985 *Nature* **313** 380

Kundu, M. R., Schmahl, E. J., Velusamy, T. and Vlahos, L., 1982 *Astron. Astrophys.*, **108** 188

Kundu, M. R., Gopalswamy, N., White, S., Cargill, P. and Schmahl, E. J., 1989 *Astrophys. J.* **347** 505

Kundu, M. R., White, S. M., Gopalswamy, N. and Lim, J., 1992 *Proc. Compton GRO Science Workshop, NASA* Publ. CP-3137

Kundu, M. R , White, S. M., Gopalswamy, N. and Lim, J., 1994 *Astrophys. J. Suppl.* **90** 599

Pneuman, G. W., 1981 *Solar Flare Magnetohydrodynamics,* ed. E. R. Priest (New York : Gordon and Breach) p 379

Ramaty, R., 1969 *Astrophys. J.* **158** 753

Ramaty, R. and Petrosian, V , 1972 *Astrophys J.* **178** 241

Sturrock, P. A., 1967 *Structure and Development of Solar Active Regions* ed. K. O. Kiepenheuer, IAU Symp. **35** 471

Tsuneta, S. *et al* (7 authors), 1992 *PASJ* **44** L63

White, S. M. and Kundu, M. R., 1992 *Solar Phys.* **141** 347